Insight: Non-Destructive Testing & Condition Monitoring,
Volume 61, Number 3, March 2019, pp. 144-148(5)
DOI:10.1784/insi.2019.61.3.144

Ultrasonic phased array inspection of a wire plus arc additive manufactured (WAAM) sample with intentionally embedded defects

Yashar Javadi[1], Charles N. MacLeod[1], Stephen G. Pierce[1], Anthony Gachagan[1], David Lines[1], Carmelo Mineo[1], Jialuo Ding[2], Stewart Williams[2], Momchil Vasilev[1], Ehsan Mohseni[1] and Riliang Su[1]

[1] *Centre for Ultrasonic Engineering (CUE), Department of Electronic & Electrical Engineering, University of Strathclyde, Glasgow G1 1XQ, UK*

[2] *Welding Engineering and Laser Processing Centre, School of Aerospace, Transport and Manufacturing Building 46, Cranfield University, Cranfield, Bedfordshire MK43 0AL, UK*

Abstract

In this study, Wire + Arc Additive Manufacture (WAAM) was employed to manufacture a steel specimen with intentionally embedded defects which were subsequently used for calibration of an ultrasonic phased array system and defect sizing. An ABB robot was used combined with the Cold Metal Transfer (CMT) Gas Metal Arc (GMA) process to deposit 20 layers of mild steel. Tungsten-carbide balls (ø1-3 mm) were intentionally embedded inside the additive structure after the 4th, 8th, 12th and 18th layers to serve as ultrasonic reflectors, simulating defects within the WAAM sample. An ultrasonic phased array system, consisting of a 5 MHz 64 Element phased array transducer, was used to inspect the WAAM sample non-destructively. The majority of the reflectors were detected successfully using Total Focusing Method (TFM), proving that the tungsten carbide balls were successfully embedded during the WAAM process and also that these are good ultrasonic reflectors. Owing to lack of standards and codes for the ultrasonic inspection of WAAM samples, a calibration method and step-by-step inspection strategy were introduced and then used to estimate the size and shape of an unknown lack of fusion (LoF) indication. This was then validated by destructive analysis, showing good correlation with the phased array results.

Keywords: Wire + Arc Additive Manufacture (WAAM); Ultrasonic Phased Array; Total Focused Method (TFM); Intentional Weld Defects.

1. Introduction

Building 3D samples by adding layer-upon-layer of material is known as Additive Manufacturing (AM), which is seeing increasing interest and use in the field of manufacturing engineering. This is driven by technical and commercial advantages in the manufacture of complex parts through more cost-effective approaches. AM can produce less material wastage,

shorter time to market, more design freedom, reduction of overall part weight and reduced complexity in comparison with the assembly and joining of many subcomponents typically deployed in other manufacturing processes [1]. However, since no single AM technique can bring all the advantages together simultaneously, it is critical to choose an AM method accurately, based on the application. The working envelope of laser and electron beam powder bed fusion limits the maximum component size [2]. This is a particular problem for the aerospace industry where the demand is for ever larger and more complex structures with lower Buy-To-Fly (BTF) ratio [1]. The necessity of reaching a lower BTF is justified by the increasing use of expensive titanium rather than aluminium (due to its electrochemical incompatibility with carbon fibre) in the aerospace industry [3]. Currently, large aircraft components (e.g., stiffened panels, wing ribs, etc.) are manufactured by machining from billets or large forgings and where a BTF ratio of 10 or even 20 is not unusual [4]. Wire + Arc Additive Manufacture (WAAM) has been successfully employed for the purpose of BTF reduction in large components [4]. For example, Williams et al [4] highlighted material savings in excess of roughly 500 kg in a 2.5 m aluminium wing rib due to a BTF reduction from 37 (traditional manufacturing methods) to 12 by WAAM at 1.1 kg/hr [4]. Regarding the deposition rate, a review on the AM methods by Ding et al [5] showed that WAAM deposition rate can reach to 12 g/min which is higher than most of the powder-based AM methods (e.g., selective laser sintering delivers just 0.1 g/min). Furthermore, WAAM has a lower capital cost in comparison with the laser and powder-based technologies, while no powder handling is required and finally a higher material usage efficiency can be achieved [6].

Non-destructive evaluation (NDE) can ensure that infrastructure owners, operators, and planners have clear and quantitative information regarding the state and condition of their asset. Skilled personnel, or emerging automated approaches, can use this information to make decisions on the remaining lifetime and required replacement, ensuring maximum asset value, usage, and safety particularly for the applications requiring inspection in the areas difficult to access and hazardous to human beings [7, 8]. This along with the increasingly demand for higher inspection accuracy and efficiency has underpinned a research and development drive to automate current NDE inspection techniques [7-9] in order to improve accuracy by reducing the weakest link in the NDE supply chain, i.e., human error [10].

As high-technology electronics are continuously delivered to the market withlower cost, it is increasingly common to use a linear array of transducers, each with its own sending and receiving electronics, rather than a single element probe [11]. In comparison with single

element transducers, ultrasonic arrays provide wider scanning areas, focusing capability, a higher inspection quality with flexibility and less inspection time due to an ability to produce a rapid visualisation. Moreover, phased array probes allow undertaking of a range of different inspections from a single location by synthetic aperture focusing and the possibility to steer the ultrasonic beam over a range of angles and positions [12-14]. The development of 2D phased-array ultrasonic imaging transducers could also increase the application of 3D volumetric imaging of components [15]. Furthermore, high-temperature arrays [16], flexible arrays [17] and air-coupled arrays [18, 19] are increasingly attractive for NDE of the components in harsh environments, particularly nuclear and aerospace industries.

As WAAM components are increasingly being considered for safety-critical industries such as aerospace, rapid development of NDE methods and structural integrity assessment of WAAM specimens is essential. This important procedure is reflected in the joint collaboration between International Organization for Standardization (ISO) and ASTM, ISO/TC 261, in which NDE for AM parts, ISO/TC 261/JG 59, which is due to be published by end of 2019 [20]. NDE for AM parts was reviewed by Clark et al [21] who highlighted that a more advanced system is required to be developed in order to accurately scan the porosities and lack-of-fusion defects between the AM layers. Lopez et al [22, 23] reviewed the application of various NDE techniques, including radiography and ultrasound, and evaluated the defect detection capability of these methods on the WAAM samples. However, they employed single element ultrasonic probes, rather than the ultrasonic array used in this paper, and surface finish was highlighted as a scanning issue in the WAAM samples [23]. The ultrasonic phased array inspection of a WAAM sample was discussed by Javadi et al [24] in aluminium.

Specimens with intentionally embedded depostion defects or flaws can be employed for training, development and research into procedures for NDE. They are more realistic and 3D representative of deposition defects, for example, a tungsten rod can represent the lack of fusion more realistically than a side-drilled hole (SDH) in the deposit [25, 26]. Furthermore, the process of the intentional deposition defect is mainly independent of the material machinability. This is beneficial for the materials which are hard to machine (e.g., Titanium) and then a suitable alternative for machining of small SDH. Tungsten carbide balls, as an example of intentional deposition defects [25], are known size defects (ø1-3 mm in this study) which can be used for calibration and sizing of the unknown size defect indications. Therefore, the tungsten carbide balls intentionally embedded in the WAAM wall are used in this study for calibration and sizing of a lack of fusion defect.

2. Theoretical background

A WAAM sample is a 3D printed specimen which is built by adding layer-upon-layer of material on a base plate using an electric arc to melt and deposit the wire, see Figure 1a. The bottom surface inspection process of the WAAM sample is schematically shown in Figure 1b. This approach was used for inspecting aluminium WAAM samples by Javadi et al [24], however, top surface inspection (see Figure 1c) has a higher potential to be used for the in-process WAAM inspection. The WAAM top surface is machined to facilitate an application of a flat-surface wedge. The probe is equipped with a standoff wedge to avoid missing near-surface reflectors due to the ultrasonic near field of the probe (Figure 1c). Assuming the presence of four artificial reflectors in the WAAM sample (Figure 1b-c) three main approaches can be used to detect these reflectors: plane B-scan, focused B-scan and Total Focusing Method (TFM), respectively represented in Figure 1d-f.

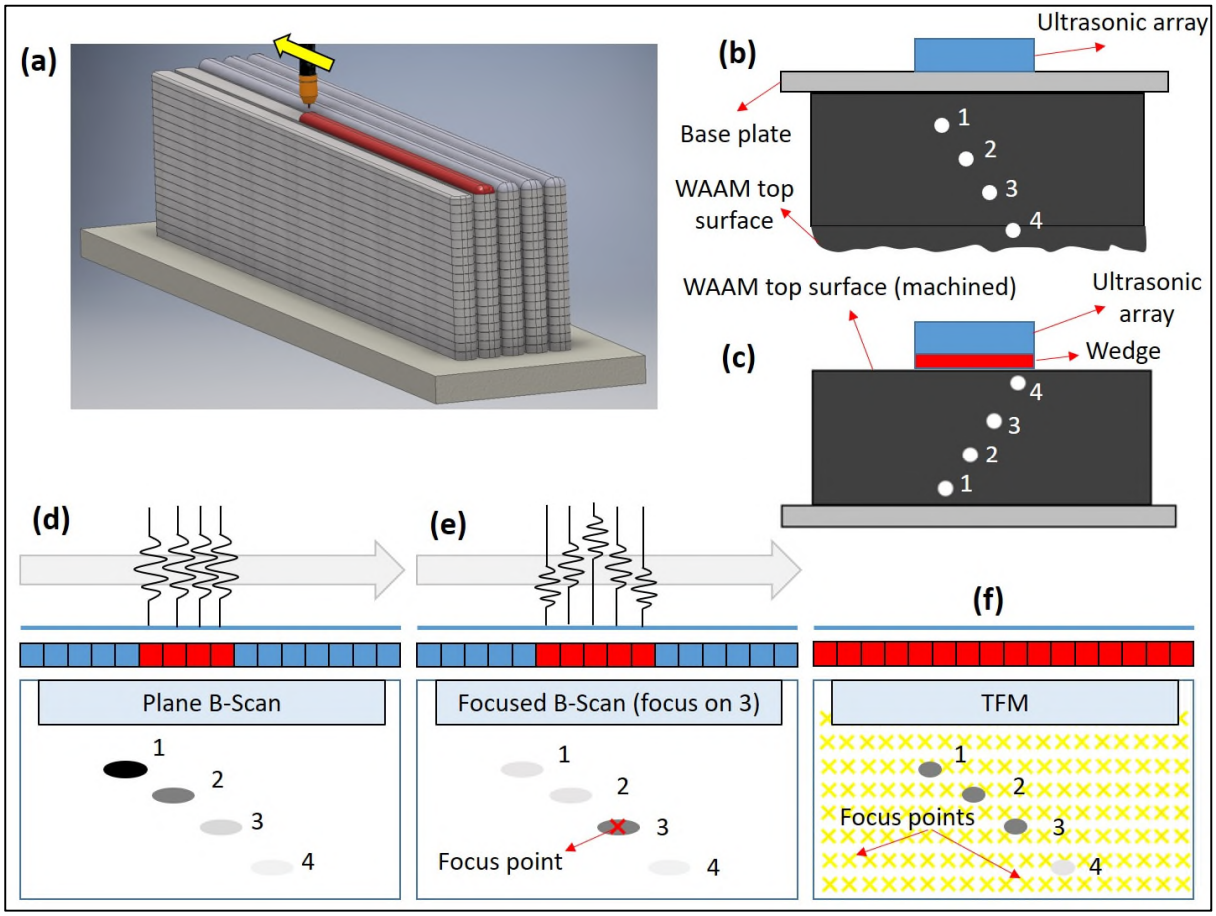

Figure 1. WAAM manufacturing process (a) and phased array inspection (b: bottom surface inspection and c: top surface inspection) using plane B-scan (d), focused B-scan (e) and TFM (f)

A B-scan (see Figure 1d) is produced using a planar front ultrasonic beam, generated by a group of adjacent elements (aperture) which are simultaneously pulsed. A single signal is then produced by summing all the echo signals (A-scans) received from the aperture elements. The performance is equivalent to a single element unfocused transducer as large as the aperture. The final B-scan image is then produced by moving the aperture electronically along the array length. Focusing can improve both sensitivity and rendition of the defect topology at the focal point. However, the beam divergence beyond the focus is increased and so a compromise value of aperture and focus is usually chosen so as to match the depth of field for the application requirements [14].

Although the focusing can help to show the defect shape more accurately, regardless of its position, it does not remove the challenges related to the penetration. Ultrasound waves are attenuated when they penetrate through the thickness of the specimen. As the WAAM specimen is a multi-layer deposition, penetrating deeper can be more challenging for the ultrasonic beam, which is required to travel through a larger number of anisotropic layers produced by multiple layers. Then, the signal-to-noise ratio reduces with the inspection depth. Therefore, a number of WAAM defects, which are positioned far from the scanning surface, can be missed. That is why the Focused B-scan (see Figure 1e) is advantageous for scanning of the deep WAAM defects. If differential time delays are introduced for the elements within an aperture at both the transmission and reception stages, a focused beam is produced [14]. However, manually setting the correct pulse delays to focus the ultrasonic energy on many points and cover the full volume of interest is time-consuming. Therefore, this paper considers the Full Matrix Capture (FMC) and Total Focusing Method (TFM) to ensure focusing for all points within the produced image (see Figure 1f). FMC involves the collection of A-scans from all elements of the array, corresponding to successive transmissions of each element, firing one at a time. This approach is used to maximise the information extracted from an array [13, 14]. TFM is an imaging algorithm that uses data acquired in FMC mode for post-processing and then all elements in the array are employed to focus at every single point in the image. The number of focal depths in transmission and reception is unlimited [14] in TFM scanning of the WAAM sample. TFM can be implemented after capturing the FMC data, off-line, or during the scanning, real-time TFM, while the latter approach requires a dedicated post-processing software as well as high computational power computer.

3. Manufacturing process (WAAM)

Figure 2 shows the manufacturing setup and the facilities for embedding intentional weld defects in the WAAM sample. The base plate was 12 mm thick and made of ground-to-bright-metal mild steel (EN 10025 S275); it was clamped in six points, as shown in Figure 2. A Gas Metal Arc (GMA) torch mounted on a six-axis ABB robot along with a cold metal transfer (CMT) power source was used. The wire was ø1.2 mm SupraMig Ultra (AWS A5.18 ER70S-6) and the shielding gas was Argoshield Light (O2 2 %; CO2 5 %; Ar 93 % - Welding mixture ISO 14175-M14-ArCO-5/2). In total, 20 layers were deposited with 5 passes in each layer. Travel speed was set in the robot program at a fixed value of 6.67 mm/s. The wire feeding speed (WFS) was set on the power source, with the possibility of adjusting it during manufacturing, without pausing the WAAM process. The WFS was 5 m/min for the 1st layer of WAAM, 4.5 m/min for the 2nd, 3rd and 4th layers but 4 m/min for all other layers. The increase in WFS of the first four layers avoids deposition defects by giving a higher heat input for the initial layers where the substrate is close

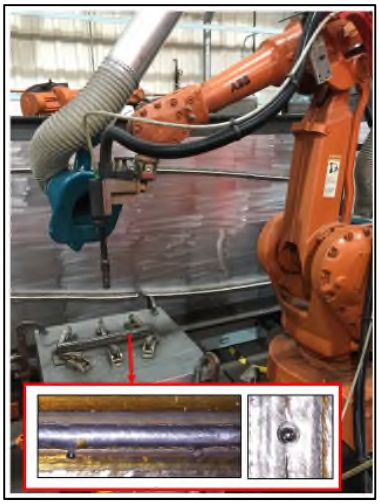

Figure 2. Manufacturing setup for the WAAM sample with the intentionally embedded tungsten carbide balls

The tungsten balls, placed inside the holes produced on the WAAM surface using a portable drilling machine, were embedded after Layer 4, 8, 12 and 18 (Figure 3).

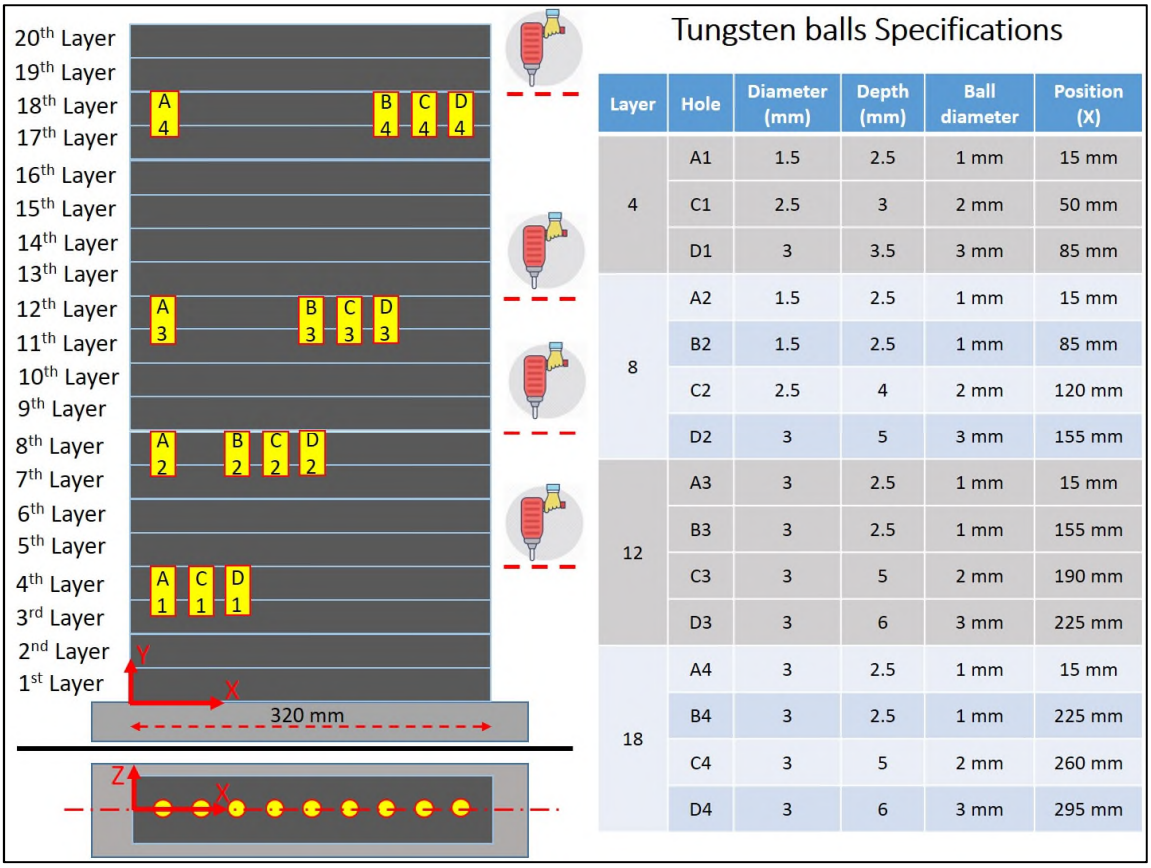

Tungsten balls Specifications

Layer	Hole	Diameter (mm)	Depth (mm)	Ball diameter	Position (X)
4	A1	1.5	2.5	1 mm	15 mm
	C1	2.5	3	2 mm	50 mm
	D1	3	3.5	3 mm	85 mm
8	A2	1.5	2.5	1 mm	15 mm
	B2	1.5	2.5	1 mm	85 mm
	C2	2.5	4	2 mm	120 mm
	D2	3	5	3 mm	155 mm
12	A3	3	2.5	1 mm	15 mm
	B3	3	2.5	1 mm	155 mm
	C3	3	5	2 mm	190 mm
	D3	3	6	3 mm	225 mm
18	A4	3	2.5	1 mm	15 mm
	B4	3	2.5	1 mm	225 mm
	C4	3	5	2 mm	260 mm
	D4	3	6	3 mm	295 mm

Figure 3. Specifications and position of the tungsten balls placement inside the WAAM sample

4. Inspection results and discussions

The ultrasonic phased array setup comprised the FIToolbox controller (Diagnostic Sonar, UK) and a 5 MHz Olympus array (64 elements 0.5mm pitch) mounted on a 20mm zero-degree Rexolite wedge (Olympus). There is no existing standard or code available for the phased array inspection of WAAM samplesFor calibration SDHs were made in the WAAM specimen (see Figure 4c). Some of the holes (ø1.5 mm and ø2 mm) are not through-holes in order to show the necessity of performing the meander scan (Figure 4d), which is discussed later. The calibration process for the ø3 mm SDH is shown in Figure 5. All the images are normalised to 80% of the maximum reflection amplitude received from the ø3 mm SDH in the S275 reference block. Therefore, any reflector with an amplitude higher than this amount appears black in colour as shown in the dB scale bar (see Figure 5). The S275 reference sample required a gain of 41 dB to bring the indication relative to the ø3 mm SDH to the black colour threshold. Although higher attenuation is expected in the WAAM sample (lower gain required in comparison with

the S275 reference sample), 35 dB gain was sufficient for WAAM specimen. This unexpected finding, due to the behaviour of the ultrasonic wave propagation inside the WAAM sample, was the main justification behind the drilling of SDHs for calibration purpose (Figure 4c). Furthermore, due to the inhomogeneous microstructure of the WAAM sample through its thickness, which includes five passes, the meander scan produces slightly different results at every scanning pass. Indeed, the gain dropped from 35 dB to 32 dB by changing the probe position in the Y direction, when scanning the through-hole reflector (see Figure 5).

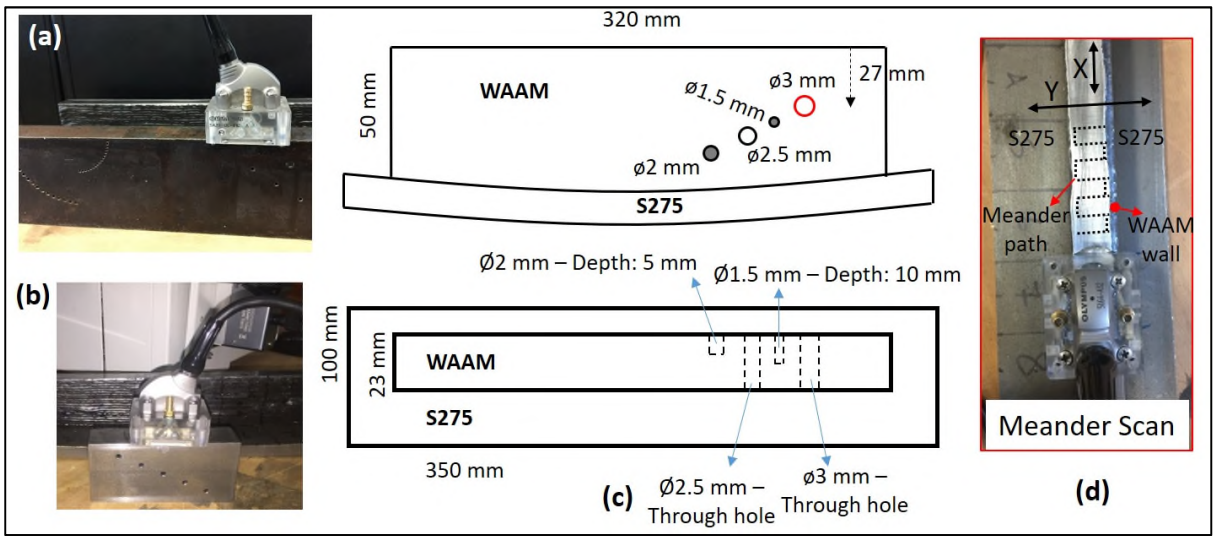

Figure 4. Ultrasonic calibration for inspection of the WAAM sample using (a) standard phased array calibration block, (b) S275 calibration sample with the same height of the WAAM sample, (c) known size SDH on the WAAM sample and (d) direction of Meander Scan

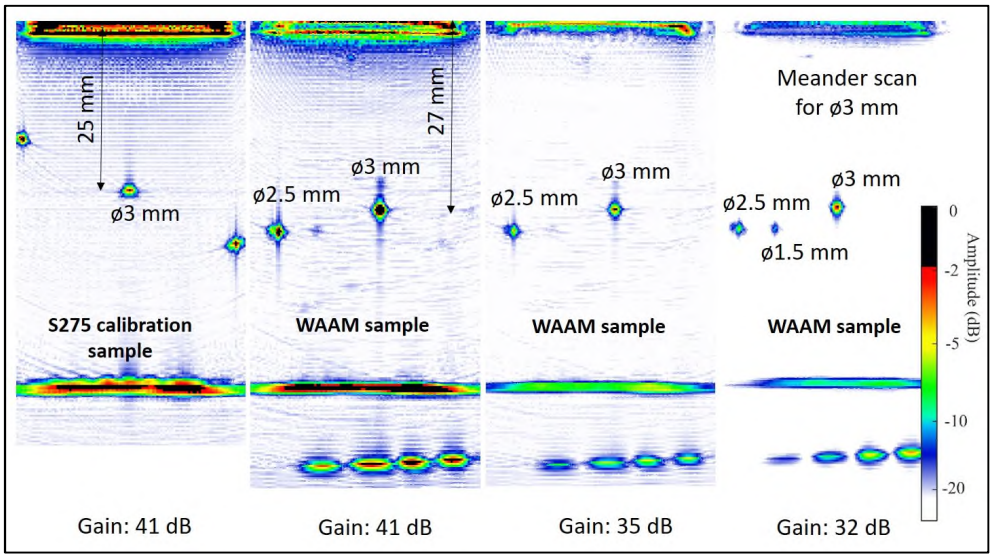

Figure 5. Calibration of ø3 mm SDH

Similarly, the meander scanning of the other SDHs on the WAAM sample was carried out and the results are summarised in Figure 6. For example, keeping the gain equal to 41 dB, if an indication breaks the black colour threshold on the UT image, it can be concluded that such defect has size equal or greater than the ø1.5 mm SDH. Then, in order to cover the full length of the whole WAAM sample, 11 consecutive sections were scanned using real-time TFM (under constant 41 dB gain). Given the array length is 30 mm, 11 sections guaranteed that the whole 320 mm WAAM wall length was swept in the X direction (Figure 7).

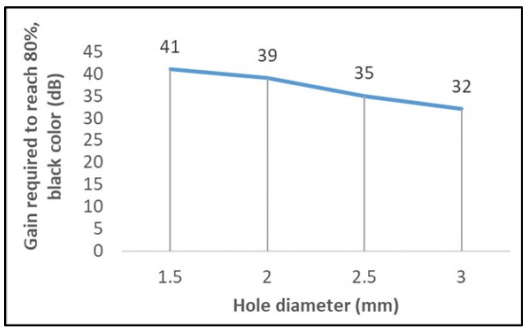

Figure 6. Calibration results: gain required to detect the SDH on the WAAM sample

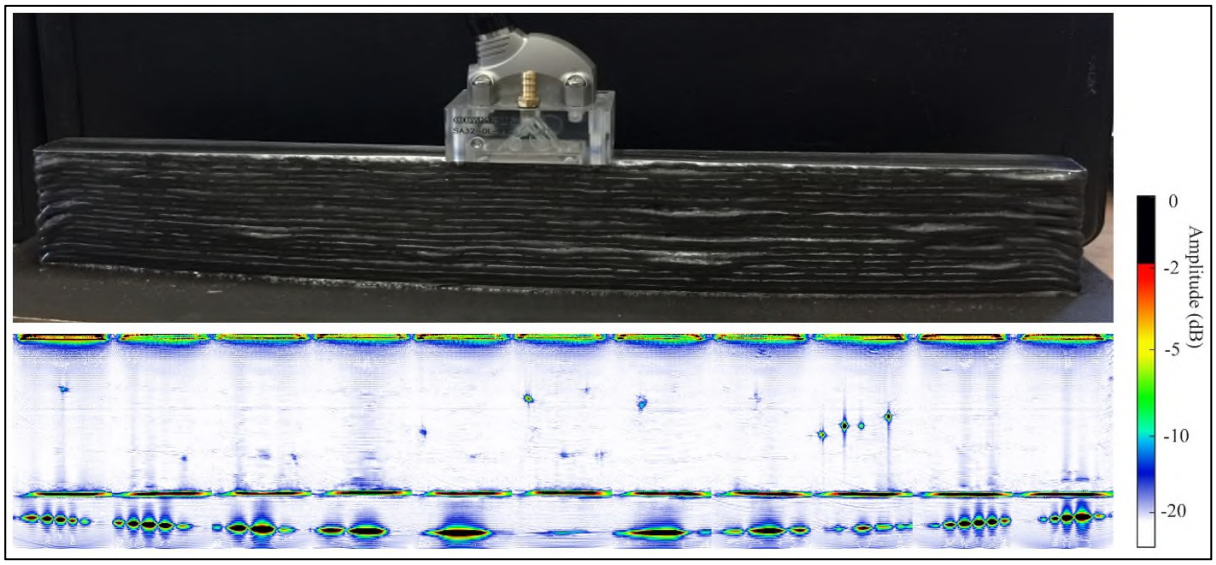

Figure 7. TFM image of the WAAM sample

The TFM images show a number of reflectors relative to the position of tungsten carbide balls. However, the TFM images are captured by moving the probe along the X direction, while keeping the centre of the wedge at the centre of the WAAM sample top surface for all 11

sections (no scanning in the Y direction). All tungsten balls should have been positioned in the WAAM wall centre during manufacturing, however both the drilling of the holes and the ball placement were manually performed. Therefore, small deviations between the final placement of the tungsten balls and the middle wall section cannot be ruled out. Meander scanning was carried out in correspondence of each reflector, in order to monitor the ultrasonic response in the Y direction (Figure 8a). The results relative to the SDHs machined in the WAAM sample and ultrasonically detected using the same gain (41 dB) are shown in Figure 8b. The gain required to reach the 80% amplitude (black colour threshold) for ø3 mm ball (D1, D2 and D3) is 53 dB (+12 dB in comparison with the reference 41 dB) as shown in Figure 8c. The required gain increment is within 7 dB and 14 dB for ø2 mm and ø1 mm balls, respectively (see Figure 8d,e). It is worth mentioning that there is a deviation between the hosting hole diameter and the ball diameter; for example, C3 was a ø2 mm ball placed in a ø3 mm hole (see Figure 3).

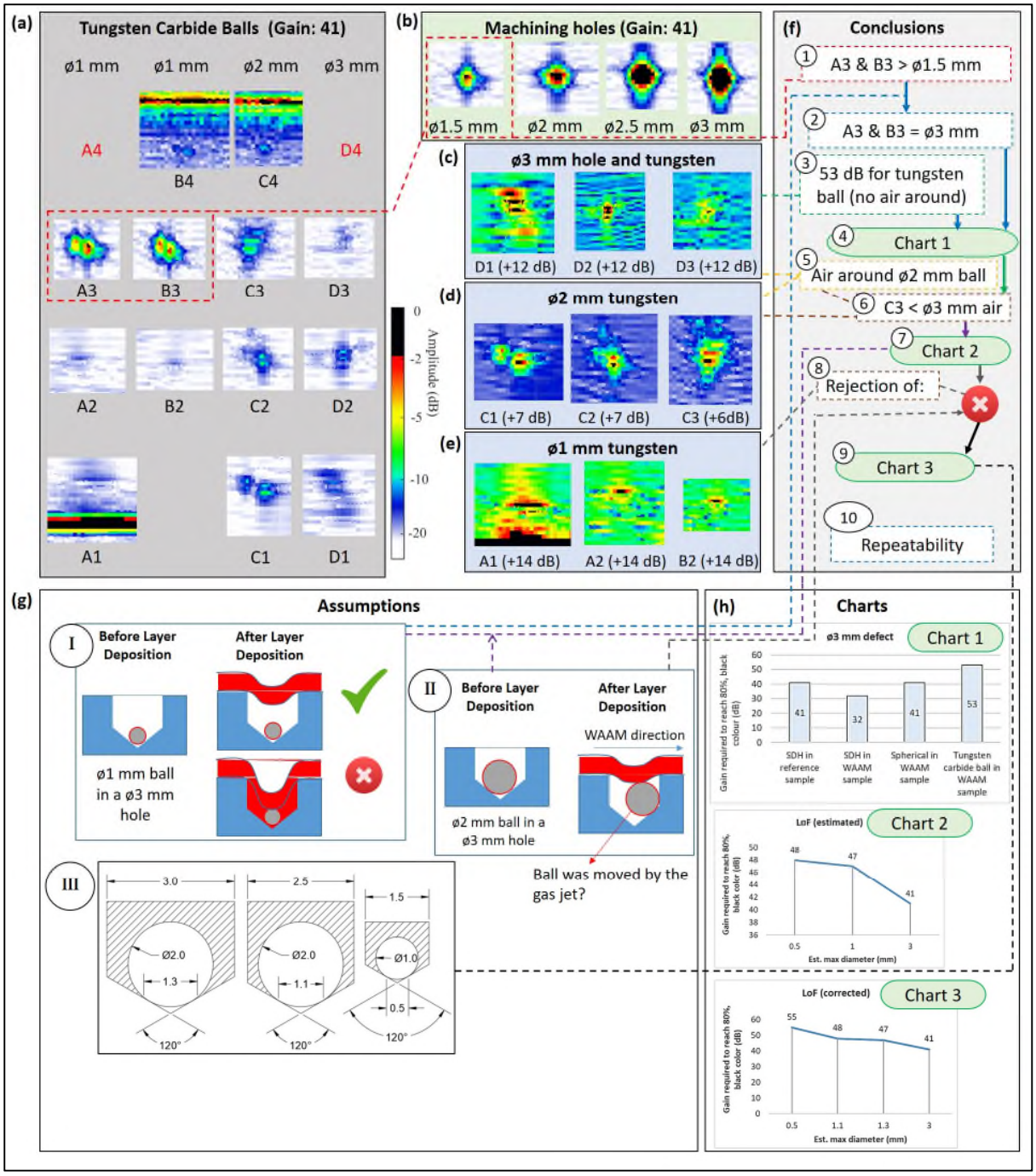

Figure 8. TFM and meander scanning results of all tungsten carbide balls (a) and SDH machined on the WAAM sample (b). The gain increase (in comparison with the reference 41 dB) required to capture black colour for (c) ø3 mm, (d) ø2 mm and (e) ø1 mm tungsten balls. Conclusions (f), assumptions (g) and summary charts (h).

The discrepancy between hole diameter and ball diameter, plus their inaccurate positions are the reasons behind a number of assumptions (Figure 8g), which support the interpretation of the results and the formulation of the conclusions listed below (the numbering refers to Figure 8f):

1) A3 and B3 are both ø1 mm balls placed in ø3 mm holes. Since the same gain (41 dB) has resulted in achieving black colour for these reflectors as well as the machining ø1.5 mm SDH, it can be concluded that A3 and B3 are ≥ ø1.5 mm (see Figure 8a,b).
2) The assumption I (see Figure 8g) is about the manufacturing process as there is uncertainty about the amount of ø3 mm hole filled by the filler wire during the deposition of the subsequent layer. There are two possibilities: (I1) the subsequent layer has quickly passed over the hole and then almost a ø3 mm hole is remained or (I2) a random amount of the hole is filled with the filler wire. It is believed that the I2 cannot be true because both A3 and B3 appear in black with exactly the same gain (41 dB) while if a random amount of air was available around the ball, this repeatability will be hard to be achieve. Furthermore, the manufacturing photographs don't show any major drop in the subsequent layer which was supposed to show a keyhole defect if the main part of the deposit had flowed inside the hole. It is then assumed that I1 is true and, therefore, the largest part of both A3 and B3 is ø3 mm. If very low amplitude of ø1 mm tungsten ball and a small melt droplet are ignored, this can be roughly considered as a ø3 mm spherical hole inside the WAAM sample which was impossible to be produced with any other manufacturing method. Therefore, a gain of 41 dB is required to detect a ø3 mm spherical hole in the WAAM sample (note this was 32 dB for a ø3 mm SDH as shown in Figure 6).
3) D1, D2 and D3 are all ø3 mm tungsten carbide balls placed in ø3 mm hole and then no air around the ball is expected.
4) The conclusion 2 and 3 plus Figure 6 results are combined in the Chart 1 (see Figure 8h) which summarised the gain required to detect different ø3 mm defect types in both WAAM and reference sample (Figure 4b).
5) Comparison between ø2 mm and ø3 mm balls shows that there is definitely some air around the ø2 mm ball, otherwise, C1-C3 required >12 dB gain increase while they are detected with just 6-7 dB (note the reflection amplitude from the air is higher than the tungsten ball).
6) C3 is a ø2 mm ball inside a ø3 mm hole but this cannot be a fully air-filled ø3 mm hole which needs just 41 dB to be detected, based on the results shown in Chart 1, rather than 41+6 dB achieved for C3. Therefore, C3 is a combination of air and tungsten plus perhaps some steel moved inside the hole during the deposition.
7) The assumption II (see Figure 8g) means that the ball is moved to the side of the hole, due to the shielding gas pressure, and then the difference between the hole diameter and

the ball diameter (0.5 mm for C1 and C2 but 1 mm for C3) is considered as the dominant air reflector in these holes. Therefore, it is required to increase the gain to 47 dB for ø1 mm LoF (air around C3) and 48 dB for ø0.5 mm LoF (air around C1-2) which results in the summary Chart 2 (see Figure 8g). It is worth mentioning that any cavity (circular or linear) filled with air, rather than filler wire or embedded tungsten balls, is considered as LoF in this work.

8) A1, A2 and B2 are all ø1 mm balls placed in ø1.5 mm hole and then, if Conclusion 7 was correct, these needed to be detected with +7 dB same as C1 and C2 which both had 0.5 mm air around the tungsten (ø2 mm ball in ø2.5 mm hole). This means that both assumption II and some part of the results in Chart 2 are incorrect.
9) Assumption III is considered in order to justify the problem discussed in conclusion 8. This assumes that the small bottom part of the hole (produced due to the drill bit shape) is blocked by the tungsten ball and then hard to be filled with the melt. This is then 1.3 mm for a ø2 mm ball placed in a ø3 mm hole and so on, see Figure 8g. Therefore, the gain required for C1 (ø2 mm ball in ø2.5 mm hole and then 0.5 mm air or LoF) which is 48 dB can be considered as the gain required for detection of 0.5 mm LoF in the WAAM sample. Similarly, the LoF size estimation can be summarised in Chart 3 (see Figure 8h).
10) Although the number of different size tungsten balls placed in different locations and inside different hole diameters resulted in a sophisticated setup, the achieved repeatability (see Figure 9) proves that this whole idea of calibration and intentional defects can obtain consistent results.

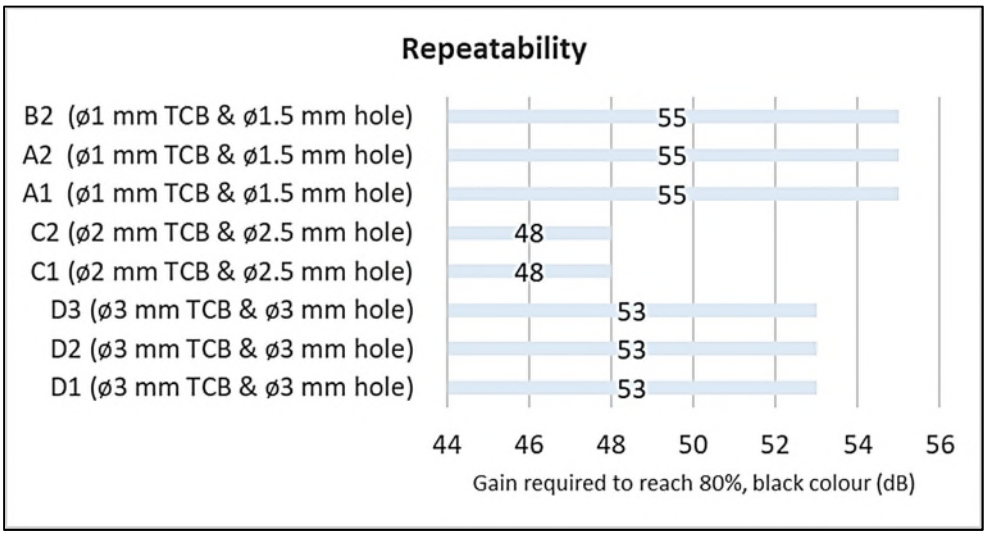

Figure 9. Repeatability achieved with the calibration procedure and intentional defects (TCB: tungsten carbide ball) used in this study

Chart 3 (Figure 8h), developed in this study, is used for the prediction of the shape and size of an unknown LoF (see Figure 10). In this work, any cavity (circular or linear) filled with air, rather than metal, is called LoF. This is however different from the standard definition of linear LoF in the desposits but it has been chosen for ease of explanation since the determination of the defect type is excluded from this paper. The unknown LoF is then assumed to have a circular cross-section in YZ plane and its diameter is considered as the size of LoF. It is also known that Chart 3 has just four points and then a linear interpolation is used to find the equivalent LoF size for the gains excluded from these points. The shape prediction and sizing are both estimated based on the calibration procedure and all discussion related to Figure 8. It was deemed critical to validate these estimations; therefore, the sample was slowly milled sidewise, with machining steps of 0.1 mm, in order to monitor the appearance of the LoF and capture its largest extension on the XZ plane. After each machining step, a ruler was placed next to the LoF and then a photo was taken. The machining results (Figure 11a) and LoF measurements are compared with the phased array ultrasonic inspection in Figure 11b. This comparison shows the length and the maximum size of the LoF had been predicted accurately. This demonstrates that the ultrasonic phased array setup and methodology used in this study is able to detect the shape and estimate the size of unknown LoF in the WAAM sample. As no calibration standard for phased array inspection of the WAAM samples exists to date; the calibration procedure developed in this study, based on intentionally embedded tungsten carbide balls, has shown potential to be used for the defect sizing in steel WAAM components.

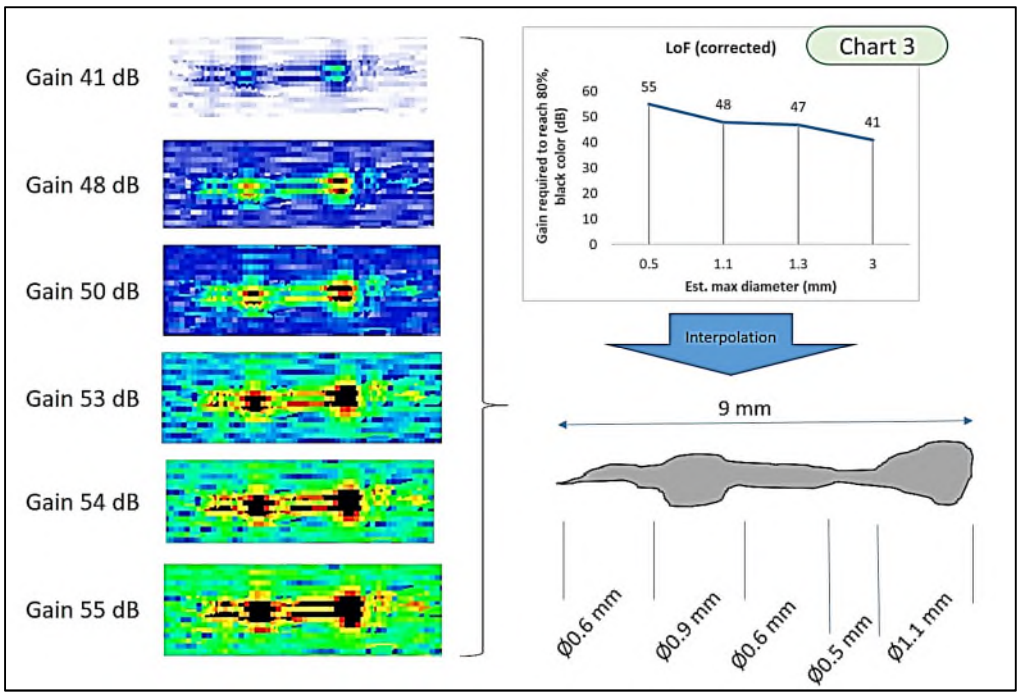

Figure 10. Sizing (estimated) of an unknown LoF using the calibration procedure developed in this study

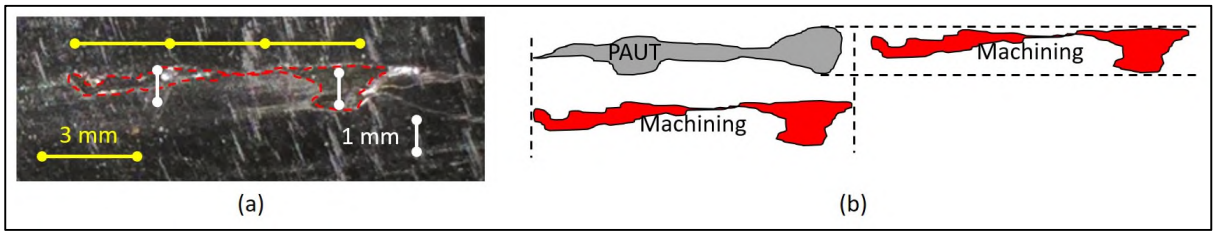

Figure 11. The LoF measurement after cutting the WAAM sample (a) and the same scale comparison of that with the phased array ultrasonic testing (PAUT) results (b)

5. Conclusions

In this study, a WAAM sample was manufactured with tungsten carbide balls intentionally embedded in the specimen. The sample was inspected using a TFM ultrasonic phased array approach. A calibration procedure was developed to enable accurate sizing of an unknown lack of fusion defect. Based on the achieved results, it can be concluded that:

1) .
2) The aforementioned lack-of-fusion defects left in the sample are supposed to be filled during the deposition of the subsequent layer. However, the ultrasonic inspection

implemented in this study shows that some of these defects are not filled which can double emphasise the necessity of the pre-heating in the WAAM process.

3) TFM was able to detect most of the defects, however, a meandering scan is required to achieve the maximum possible amplitude for the reflectors.
4) The ultrasonic phased array system was calibrated using SDH machined in the WAAM wall.
5) Owing to the variation in the tungsten balls diameter, location and the drilled hole diameter, a step-by-step methodology is developed to achieve a chart for sizing of an unknown defect in the steel WAAM specimen.
6) Using the developed relationship between the defect size and the gain, shape and size of an unknown LoF was detected and a reasonable agreement was achieved when the inspection results were compared with the actual defect dimensions measured on the WAAM machined surface.
7) Because the methodology used here is validated, the assumptions made are considered as verified assumptions and then it can be claimed that a number of known size tungsten balls and known size near-spherical air-filled defects were successfully embedded in the WAAM wall using an intentional defect process. From a manufacturing point of view, embedding a known size air-filled defect is impractical with the other manufacturing methods. This shows the value of intentional defect process discussed here.
8) In comparison with the ø3 mm spherical air-filled defect, the ø3 mm tungsten carbide ball was detected with +12 dB gain increase. This proves that the tungsten carbide balls, if they are successfully embedded during the WAAM process, are good reflectors of the ultrasonic wave and subsequent detection of them plus the controlled air-filled defects around them can also be beneficial for the NDE calibration and sizing purposes.

Finally, a comprehensive inspection strategy has been tested to detect and size steel WAAM defects. It is recommended to focus future work on the development of the same strategy for other WAAM materials (e.g. titanium) and for different additive manufacturing processes. Although CMT was used here, ultrasonic defect detection on samples produced with other methods (e.g. Laser metal deposition or plasma transferred arc WAAM) is worth studying in the future works.

6. Acknowledgements

This work is supported by an EPSRC project (EP/P031064/1) called Robotic Wire + Arc Additive Manufacture (RoboWAAM). The authors then like to acknowledge EPSRC for the support and funding the project.

7. References

[1] J. Coykendall, M. Cotteleer, J. Holdowsky, M. Mahto, 3D opportunity in aerospace and defense: additive manufacturing takes flight, A Deloitte series on additive manufacturing, Deloitte University Press, Westlake, TX, 2014.
[2] W.E. Frazier, Metal Additive Manufacturing: A Review, Journal of Materials Engineering and Performance 23 (2014) 1917-1928.
[3] C. Vargel, Corrosion of Aluminium, Elsevier Ltd., Oxford, 2004.
[4] S.W. Williams, F. Martina, A.C. Addison, J. Ding, G. Pardal, P. Colegrove, Wire plus Arc Additive Manufacturing, Materials Science and Technology 32 (2016) 641-647.
[5] D.H. Ding, Z.X. Pan, D. Cuiuri, H.J. Li, Wire-feed additive manufacturing of metal components: technologies, developments and future interests, International Journal of Advanced Manufacturing Technology 81 (2015) 465-481.
[6] F.D. Wang, S. Williams, P. Colegrove, A.A. Antonysamy, Microstructure and Mechanical Properties of Wire and Arc Additive Manufactured Ti-6Al-4V, Metallurgical and Materials Transactions a-Physical Metallurgy and Materials Science 44A (2013) 968-977.
[7] C.N. Macleod, G. Dobie, S.G. Pierce, R. Summan, M. Morozov, Machining-Based Coverage Path Planning for Automated Structural Inspection, Ieee Transactions on Automation Science and Engineering 15 (2018) 202-213.
[8] G. Dobie, R. Summan, S.G. Pierce, W. Galbraith, G. Hayward, A Noncontact Ultrasonic Platform for Structural Inspection, Ieee Sensors Journal 11 (2011) 2458-2468.
[9] R.S. Lim, H.M. La, W.H. Sheng, A Robotic Crack Inspection and Mapping System for Bridge Deck Maintenance, Ieee Transactions on Automation Science and Engineering 11 (2014) 367-378.
[10] P.A. Hancock, M.H. Chignell, MENTAL WORKLOAD DYNAMICS IN ADAPTIVE INTERFACE DESIGN, Ieee Transactions on Systems Man and Cybernetics 18 (1988) 647-658.
[11] P. Cawley, Non-destructive testing - current capabilities and future directions, Proc. Inst. Mech. Eng. Pt. L-J. Mater.-Design Appl. 215 (2001) 213-223.
[12] B.W. Drinkwater, P.D. Wilcox, Ultrasonic arrays for non-destructive evaluation: A review, Ndt & E International 39 (2006) 525-541.
[13] C. Holmes, B.W. Drinkwater, P.D. Wilcox, Advanced post-processing for scanned ultrasonic arrays: Application to defect detection and classification in non-destructive evaluation, Ultrasonics 48 (2008) 636-642.
[14] C. Holmes, B.W. Drinkwater, P.D. Wilcox, Post-processing of the full matrix of ultrasonic transmit-receive array data for non-destructive evaluation, Ndt & E International 38 (2005) 701-711.
[15] Y. Mendelsohn, E. Wiener-Avnear, Simulations of circular 2D phase-array ultrasonic imaging transducers, Ultrasonics 39 (2002) 657-666.
[16] K.J. Kirk, A. McNab, A. Cochran, I. Hall, G. Hayward, Ultrasonic arrays for monitoring cracks in an industrial plant at high temperatures, Ieee Transactions on Ultrasonics Ferroelectrics and Frequency Control 46 (1999) 311-319.

[17] S. Chatillon, G. Cattiaux, M. Serre, O. Roy, Ultrasonic non-destructive testing of pieces of complex geometry with a flexible phased array transducer, Ultrasonics 38 (2000) 131-134.
[18] A. Neild, D.A. Hutchins, T.J. Robertson, L.A.J. Davis, D.R. Billson, The radiated fields of focussing air-coupled ultrasonic phased arrays, Ultrasonics 43 (2005) 183-195.
[19] A. Gachagan, S. Kelly, M. Altman, E. Grauvogl, G. Hayward, R. Banks, T. McCunnie, D. Skillen, Development of a manual air-coupled ultrasonic inspection instrument for use on aeronautical structures under in-service conditions, Review of Progress in Quantitative Nondestructive Evaluation, Vols 22a and 22b 20 (2003) 883-890.
[20] C.-P. Bazin de Caix, A. Gigant, ISO/TC 261: Additive manufacturing, in: B. Dutton (Ed.) NDT for AM parts, International Organization for Standardization, 2018.
[21] D. Clark, S.D. Sharples, D.C. Wright, Development of online inspection for additive manufacturing products, Insight 53 (2011) 610-613.
[22] A. Lopez, R. Bacelar, I. Pires, T. Santos, L. Quintino, MAPPING OF NON-DESTRUCTIVE TECHNIQUES FOR INSPECTION OF WIRE AND ARC ADDITIVE MANUFACTURING, Proceedings of the 7th International Conference on Mechanics and Materials in Design (M2d2017) (2017) 1829-1844.
[23] A. Lopez, R. Bacelar, I. Pires, T.G. Santos, J.P. Sousa, L. Quintino, Non-destructive testing application of radiography and ultrasound for wire and arc additive manufacturing, Additive Manufacturing 21 (2018) 298-306.
[24] Y. Javadi, C.N. MacLeod, S.G. Pierce, A. Gachagan, W. Kerr, J. Ding, S. Williams, M. Vasilev, R. Su, C. Mineo, J. Dziewierz, Ultrasonic phased array inspection of wire plus arc additive manufacture (WAAM) samples using conventional and total focusing method (TFM) imaging approaches, Insight 61 (2019) 144-148.
[25] Y. Javadi, M. Vasilev, C.N. MacLeod, S.G. Pierce, R. Su, C. Mineo, J. Dziewierz, A. Gachagan, Intentional weld defect process : from manufacturing by robotic welding machine to inspection using TFM phased array, 45th Annual Review of Progress in Quantitative Nondestructive Evaluation., AIP, Burlington, United States, 2018.
[26] M. Consonni, C.F. Wee, C. Schneider, Manufacturing of welded joints with realistic defects, Insight 54 (2012) 76-+.

2019-03-01

Ultrasonic phased array inspection of wire plus arc additive manufacture samples using conventional and total focusing method imaging approaches

Javadi, Yashar

British Institute of Non-destructive Testing

Javadi Y, MacLeod CN, Pierce SG, et al., (2019) Ultrasonic phased array inspection of wire plus arc additive manufacture samples using conventional and total focusing method imaging approaches. Insight: Non-Destructive Testing & Condition Monitoring, Volume 61, Issue 3, 2019, pp. 144-148

https://doi.org/10.1784/insi.2019.61.3.144